

A measure of cosmological distance using the C IV Baldwin effect in quasars

Long Huang^{1,2*}, Hui Wang³, Zhifu Gao⁴, Xiangyun Zeng⁵, Zhangyong Chang^{1,2}

¹ College of Science, Jiujiang University, Jiujiang 332000, People's Republic of China

² Key Laboratory of Functional Microscale Materials in Jiangxi Province, Jiujiang 332000, People's Republic of China

³ School of Physics and Astronomy, China West Normal University, Nanchong 637000, People's Republic of China

⁴ Xinjiang Astronomical Observatory, Chinese Academy of Sciences, Urumqi 830011, People's Republic of China

⁵ College of Science, China Three Gorges University, Yichang 443000, People's Republic of China

July 11, 2023

ABSTRACT

We use the anticorrelation between the equivalent width (EW) of the C IV 1549 Å emission line and the continuum luminosity in the quasars rest frame (Baldwin effect) to measure their luminosity distance as well as estimate cosmological parameters. We obtain a sample of 471 Type I quasars with the UV-optical spectra and EW (C IV) measurements in the redshift range of $2.3 < z < 7.1$ including 25 objects at $5 < z < 7.1$, which can be used to investigate the C IV Baldwin effect and determine cosmological luminosity distance. The relation $EW(C\text{ IV}) \propto (\lambda L_\lambda)^7$ can be applied to check the inverse correlation between the C IV EW and L_λ of quasars and give their distance, and the data suggest that the EW of C IV is inversely correlated with continuum monochromatic luminosities. On the other hand, we also consider dividing the Type I quasar sample into various redshift bins, which can be used to check if the C IV EW-luminosity relation depends on the redshift. Finally, we apply a combination of Type I quasars and Type Ia supernovae (SNIa) of the Pantheon sample to test the property of dark energy concerning whether or not its density deviates from the constant, and give the statistical results.

Key words. Quasars; quasars: emission lines; Cosmology; Dark energy

1. Introduction

A wide variety of emission line strengths and velocity widths are the important spectral features of active galactic nuclei (AGNs) and quasars, which can be used to classify these objects and investigate the correlation between the equivalent widths (EWs) of emission lines and continuum luminosities in the UV-optical band. The full width at half maximum (FWHM) of the emission lines often involves the orientation relative to the line of sight (Shen & Ho 2014). Broad lines are defined as having $FWHM \approx 1000 - 15,000 \text{ km s}^{-1}$ and narrow lines as $FWHM \approx 200 - 2000 \text{ km s}^{-1}$ (Sulentic et al. 2000). On this basis, AGNs and quasars can be categorized by whether they have broad emission lines (Type I), only narrow lines (Type II), or no lines except when a variable continuum is in a low phase (Blazars) (Urry & Padovani 1995; Sulentic et al. 2000). In addition, other classification methods of quasars can be based on the ratio of monochromatic luminosities. Radio-loud quasars satisfy $\log R > 1$ and radio-quiet quasars with $\log R \leq 1$, where R is the ratio of monochromatic luminosities (with units of $\text{erg} \cdot \text{s}^{-1} \cdot \text{Hz}^{-1}$) measured at (rest-frame) 5GHz and 2500 Å (Strittmatter et al. 1980; Kellermann et al. 1989; Stocke et al. 1992; Kellermann et al. 1994).

On the other hand, the correlation between the equivalent width (EW) of the C IV 1549 Å emission line and the continuum luminosity in the quasars rest frame was in-

vestigated by Baldwin (Baldwin 1977). The data suggested that the C IV EW anticorrelates with continuum monochromatic luminosities based on a sample of 20 quasars in the redshift range $1.24 \leq z \leq 3.53$. This has become known as the Baldwin effect (hereafter BEff). Subsequently, more spectroscopic data of AGNs and quasars are used to verify the BEff, and it exists not only for C IV but also for many other UV-optical emission lines such as $\text{Ly}\alpha$ $\lambda 1215.7$, $\text{C III}]$ $\lambda 1908.7$, Mg II $\lambda 2800.3$ (Kinney et al. 1990; Netzer et al. 1992; Croom et al. 2002). Although the physical reason for the BEff remains unknown, there are several explanations that try to account for the UV-optical BEff.

One promising explanation is the softening of the spectral energy distribution (SED) that the soft X-ray continuum between 0.1 and 1keV in high-luminosity quasars is weaker than that in low-luminosity AGNs, which determines the heating rate and the excitation of various collisionally excited lines (Netzer et al. 1992; Zheng et al. 1995; Dietrich et al. 2002). It is an important clue for the physical cause of the UV-optical BEff. Other underlying physical causes of the BEff involve the black hole mass (Xu et al. 2008; Chang et al. 2021), the Eddington ratio L/L_{Edd} (Baskin & Laor 2004; Xu et al. 2008; Dong et al. 2009; Nikolaïjuk & Walter 2012; Shemmer & Lieber 2015), and the luminosity dependence of metallicity (Dietrich et al. 2002; Sulentic et al. 2007).

In this paper we introduce the source of data used in Section 2, including the EW of the C IV 1549 Å emission line, and the continuum luminosity at 2500 Å of 471 Type

* e-mail: huanglong20122021@163.com

I quasars. In Section 3 we employ the nonlinear relation $EW(C\text{IV}) \propto (\lambda L_{2500\text{\AA}})^\gamma$ to check the correlation between the C IV EW and continuum luminosity of Type I quasars, and give their cosmological luminosity distance. In Section 4 we consider dividing the Type I quasar sample into various redshift bins, which can be used to check if the C IV EW-luminosity relation depends on the redshift. In Section 5, we apply a combination of Type I quasars and SNIa Pantheon to reconstruct the dark energy equation of state $w(z)$, which can be used to test the nature of dark energy concerning whether or not its density deviates from the constant. In Section 6, we summarize the paper.

2. Data used

Modern optical instruments and surveys including the Sloan Digital Sky Survey (SDSS) (Lyke et al. 2020; Ahumada et al. 2020), the Hubble Space Telescope (HST) (Tacconi et al. 2018), and the International Ultraviolet Explorer (IUE) provide the UV-optical spectra for a large amount of quasars (Kondo et al. 1989), which can be used to investigate the C IV BEff. Alam et al. (2015) presented the Data Release 12 Quasar catalog (DR12) data gathered by SDSS-III from 2008 August to 2014 June, which includes the spectra of 294,512 quasars (Alam et al. 2015). Their emission line fluxes or EWs and widths can be measured by different techniques, and sometimes different results are obtained for the same set of data (Berk et al. 2001; Shen et al. 2008, 2011; Shen & Ménard 2012; Pâris et al. 2011, 2012).

We introduce two main calculation methods for the flux and width of emission lines. The first is to use two Gaussian functions to fit the emission-line spectrum given after subtracting the power-law continuum ($f_\nu \propto \nu^{\alpha_\nu}$). The second method is to employ the principal component analysis (PCA) method to estimate continuum spectrum; this employs the assumption that the covariance matrix of the entire sample can be considered as the covariance matrix of the single sample. Using PCA to fit the continuum and emission line avoids the need to assume a line profile in a region of the spectrum affected by sky subtraction.

We use two Gaussian functions to fit C IV and C III] emission lines with the fitting window 1450-1700 Å and 1800-2000 Å in the rest frame, and the weak emission line He II is not taken into account. The width and amplitude are independent parameters, but the two Gaussians are bound to have the same emission redshift. Figure 2 shows the corresponding C IV emission line fit from a two-Gaussian fit. Meanwhile, the PCA method is also applied to fit the spectra. Examples of fitting results for the power-law and Gaussian method and the PCA method are presented in Fig. 1. The C IV EW from the two-Gaussian fit is larger than the measurement from the PCA method, and the power-law and Gaussian method gives simpler results to the PCA method, so we consider using the EW of emission lines obtained by the PCA method to study C IV BEff. Pâris et al. (2017) provided the various measured quantities of 297 301 quasars from DR12 based on the result of a PCA of the spectra. Therefore, we filter samples from their released data to check the correlation between the C IV EW and the continuum luminosity for quasars and measure their cosmological luminosity distance.

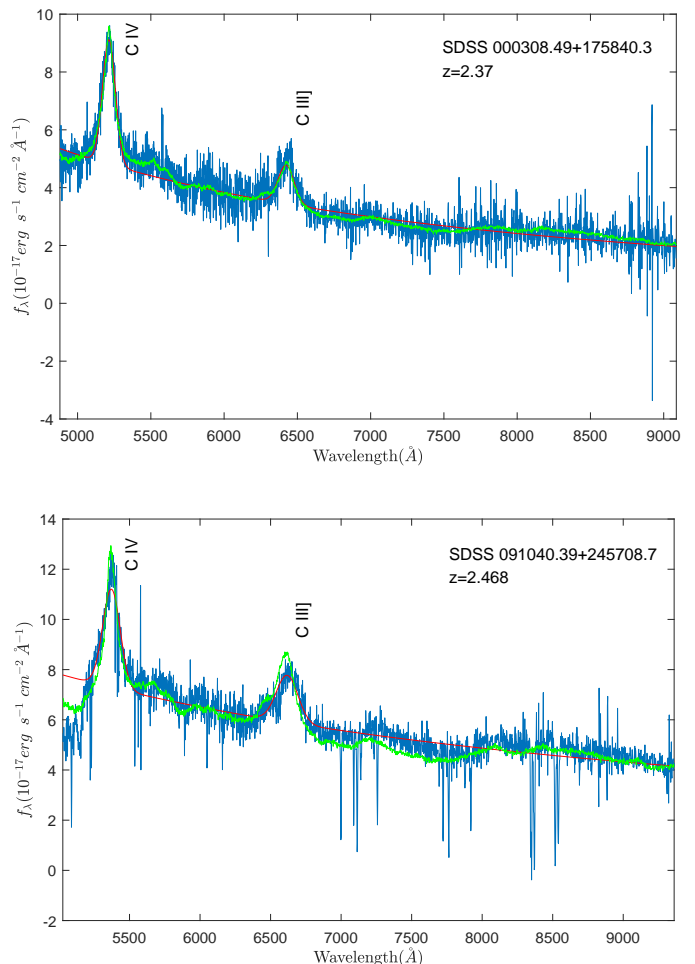


Fig. 1: Illustration of two methods used to fit continuum and emission lines. The red line is a fit of the power-law continuum and two Gaussians functions for C IV and C III] emission lines; the green line is the PCA estimate of the continuum.

3. Parameter constraints from Type I quasars

3.1. Insights from scatter plots

The linear formula is usually used to investigate the correlation between the C IV EW and λL_λ for quasars, which can be written as

$$\log EW(C\text{IV}) = \beta + \gamma \log(\lambda L_\lambda(2500\text{\AA})). \quad (1)$$

This equation is equivalent to the relation $EW(C\text{IV}) \propto (\lambda L_{2500\text{\AA}})^\gamma$. We fitted equation (1) to 8630 Type I quasars and obtained the residual $\Delta(\log EW(C\text{IV}))$ from the statistical values of β and γ ; the luminosities $L_\lambda(2500\text{\AA})$ were obtained from the measured fluxes assuming Λ CDM cosmology ($\Omega_m = 0.3$, $H_0 = 70 \text{ km s}^{-1} \text{ Mpc}^{-1}$). The $\log EW(C\text{IV}) - L_{UV}$ plot of Type I quasars are shown in the upper panel of Fig. 3; the lower panel of Fig. 3 illustrates $\Delta(\log EW(C\text{IV}))$ against L_{UV} , which implies that the BEff slope γ is dependent on luminosity. We also analyzed the $\Delta(\log EW(C\text{IV})) - \Gamma_{UV}$ relation and investigate the correlation between the luminosity L_{UV} and the UV-optical power-law index Γ_{UV} , Γ_{UV} can be obtained from a fit of $f_\nu \propto \nu^{-(\Gamma_{UV}-1)}$ to u, g, r, i and z

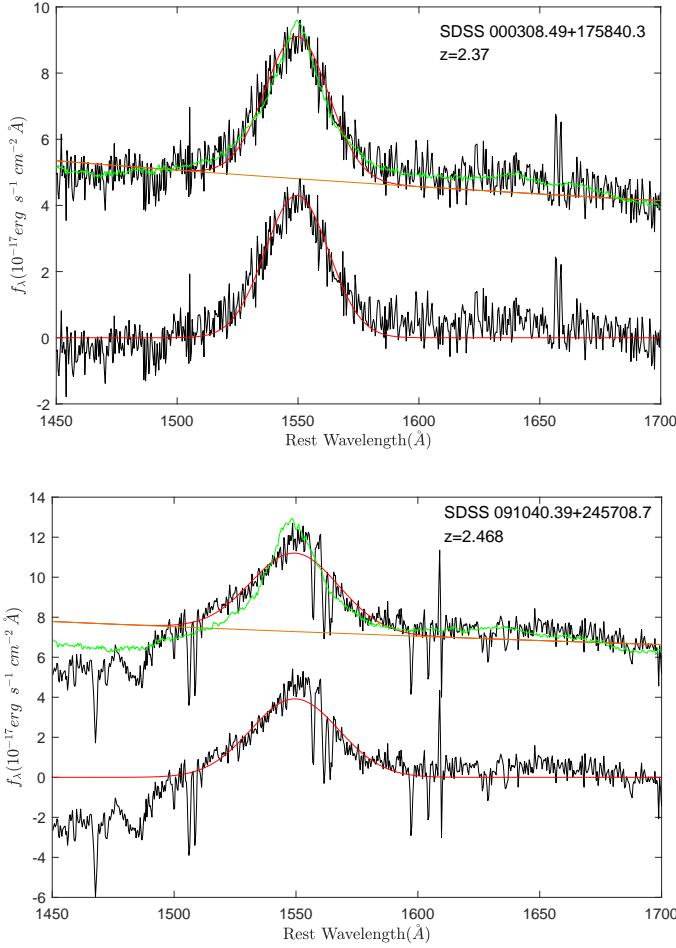


Fig. 2: Two examples of continuum and C IV emission line fit. In each panel the upper black solid line is the original and the lower black solid line is continuum subtracted; the red and green solid curves are the fits to the spectra by Gaussian fit and PCA method; the orange lines show the fitted power-law continuum.

band. The index Γ_{UV} of Type I quasars with $z > 3$ seem to be inapplicable to study a corresponding correlation and needs to be excluded. The residual $\Delta(\log EW(C\text{IV}))$ against Γ_{UV} for Type I quasars with $z \leq 3$ is shown in the upper panel of Fig. 4; it implies that $\Delta(\log EW(C\text{IV}))$ has no dependence on Γ_{UV} . The luminosity L_{UV} against Γ_{UV} is provided in the lower panel of Fig. 4; their correlation coefficient is $r = 0.131$, which indicates that the luminosity L_{UV} might be weakly correlated with the UV-optical power-law index Γ_{UV} .

3.2. Filter data for measuring luminosity distance

As can be seen in the lower panel of Fig. 3, the luminosity dependence of the BEff slope is indicated for a large number of samples, so we fitted our data points with $45.8 \leq \log(\lambda L_\lambda(2500\text{\AA})) \leq 46.5$ to avoid the luminosity dependence for γ . Meanwhile, in order to reduce the dispersion, we select the sample at $z \leq 3$ by $\sigma(EW)/EW(C\text{IV}) < 0.02$, $\sigma(EW)/EW(C\text{IV}) < 0.023$ for $3 < z \leq 5$, $\sigma(EW)$ is the uncertainty for $EW(C\text{IV})$, and the higher redshift $z > 5$ with $\sigma(EW)/EW(C\text{IV}) < 0.06$, which ensures that the

numbers of objects are close in different redshift bins. We then obtain a sample of 471 Type I quasars ($2.3 < z < 7.1$). We also match the sample to the latest FIRST catalog and The NRAO VLA sky survey (NVSS) data using a $2''$ matching radius (Helfand et al. 2015; Condon et al. 1998), only about 20 objects have FIRST and NVSS counterparts, but all of them satisfy $\log R > 1$, these radio-loud sources and other quasars compose a total sample of 471 Type I quasars. We can use this sample to investigate BEff and calculate the luminosity distance.

3.3. Parametric formula for C IV EW and the continuum flux

Using relation $L = 4\pi D_L^2 f$ in equation (1), we get

$$\log EW(C\text{IV}) = \Phi(\lambda f_\lambda(2500\text{\AA}), D_L) = \beta + \gamma \log(\lambda f_\lambda(2500\text{\AA})) + \gamma \log(4\pi D_L^2), \quad (2)$$

where $f_\lambda(2500\text{\AA})$ is the flux measured at (rest-frame) 2500\AA ; $EW(C\text{IV})$ is the equivalent width of the C IV 1549\AA emission line; and D_L is the luminosity distance, which depends on the redshift z . Thus, equation (2) can be used to check the C IV EW-luminosity correlation for Type I quasars and determine their cosmological luminosity distance.

We fit the C IV EW-luminosity relation to Type I quasars by minimizing a likelihood function consisting of a modified χ^2 function based on a Markov chain Monte Carlo (MCMC) function, allowing for an intrinsic dispersion δ

$$-2 \ln L = \sum_{i=1}^N \left\{ \frac{[\log EW(C\text{IV})_i - \Phi(\lambda f_\lambda(2500\text{\AA}), D_L)_i]^2}{s_i^2} \right\} + \sum_{i=1}^N \ln(2\pi s_i^2), \quad (3)$$

where $\Phi(\lambda f_\lambda(2500\text{\AA}), D_L)_i$ is given by equation (2) and $s_i^2 = \sigma_i^2(\log EW(C\text{IV})) + \gamma^2 \cdot \sigma_i^2(\log(\lambda f_\lambda(2500\text{\AA}))) + \delta^2$; $\sigma_i(\log EW)$ and $\sigma_i(\log(\lambda f_\lambda(2500\text{\AA})))$ indicate the statistical errors for $\log EW(C\text{IV})$ and $\log(\lambda f_\lambda(2500\text{\AA}))$; and δ is the intrinsic dispersion (Kim 2011; Risaliti & Lusso 2015), which can be fitted as a free parameter.

We do not consider the large positive and negative space curvature as they have not been obviously observed by observational data, and we approximately adopt a curvature of $\Omega_k = 0$; a prior cosmological constant Λ CDM model is assumed, then $\Omega_\Lambda = 1 - \Omega_m$ when $\Omega_R \ll \Omega_m$. In this case the free parameters are β , γ and the intrinsic dispersion δ , and the cosmological parameters Ω_m . We note that the Hubble constant H_0 is absorbed into the parameter β when fitting equation (2), without an independent determination of this parameter, so we fix $H_0 = 70 \text{ km s}^{-1} \text{ Mpc}^{-1}$ (Reid et al. 2019; Aghanim et al. 2020).

Meanwhile, we measure the distance modulus for Type I quasars based on the C IV EW-luminosity relation. On the other hand, other methods for quasars also can be applied to measure their luminosity distance (La Franca et al. 2014; Risaliti & Lusso 2015; Martínez-Aldama et al. 2019; Dultzin et al. 2020). Equation (2) gives the distance modulus as

$$DM = \frac{5[\log EW(C\text{IV}) - \gamma \log(\lambda f_\lambda(2500\text{\AA})) - \beta']}{2\gamma} + 25, \quad (4)$$

where $\beta' = \beta + \gamma \log(4\pi)$. The error is

$$\sigma_{DM} = DM \sqrt{\left(\frac{\sigma_f}{f}\right)^2 + \left(\frac{\sigma_\gamma}{\gamma}\right)^2}, \quad (5)$$

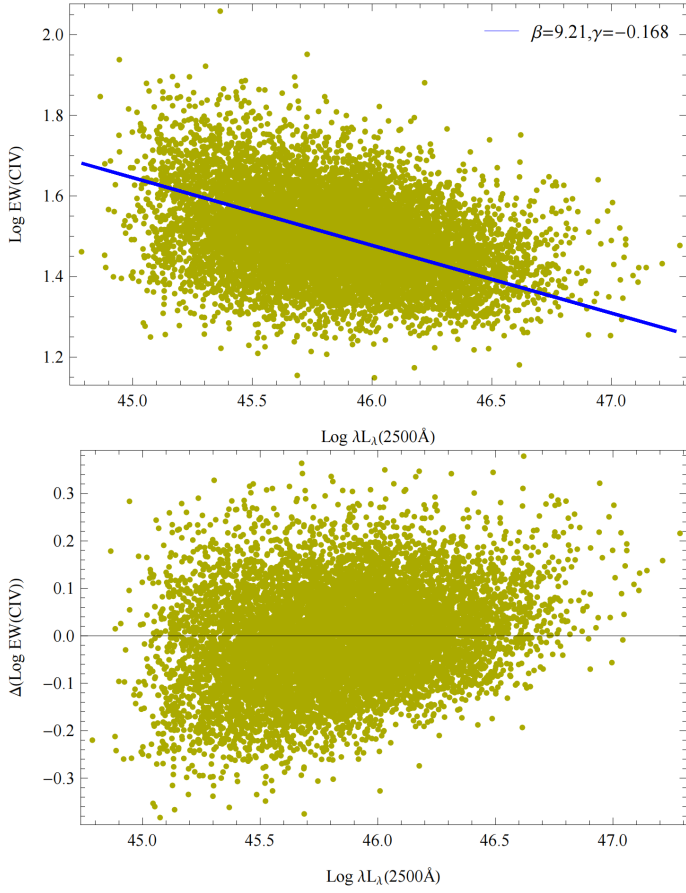


Fig. 3: Plot of $\log EW(C\text{ IV})$ vs. L_{UV} (upper panel), $\Delta(\log EW(C\text{ IV}))$ vs. L_{UV} (lower panel) for Type I quasars. The blue line in the upper panel is the theoretical values of $\log EW(C\text{ IV})$ from Eq. (1) with the best fitting values of β and γ . $\Delta(\log EW(C\text{ IV}))$ represents the residuals from the subtraction of the observational data and theoretical values. In the lower panel the relationship between $\Delta(\log EW(C\text{ IV}))$ and L_{UV} indicates the luminosity dependence of the BEff slope.

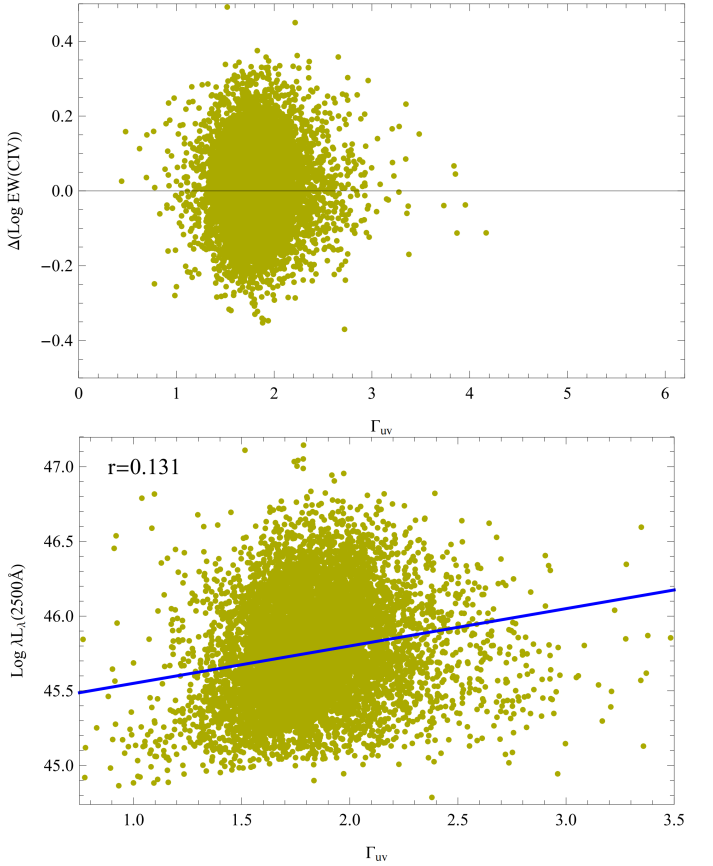


Fig. 4: Plot of $\Delta(\log EW(C\text{ IV}))$ vs. Γ_{UV} (upper panel) and L_{UV} vs. Γ_{UV} (lower panel) for Type I quasars with $z \leq 3$, where Γ_{UV} is the UV-optical power-law index, and r represents the correlation coefficient.

where $f = \log EW(C\text{ IV}) - \gamma \log(\lambda f_\lambda(2500 \text{ \AA})) - \beta'$, and $\sigma_f^2 = \sigma^2(\log EW(C\text{ IV})) + \gamma^2 \cdot \sigma^2(\log(\lambda f_\lambda(2500 \text{ \AA}))) + \sigma_{\beta'}^2$. From equation (5), the uncertainty of the slope of the BEff γ obviously influences the error of distance modulus for Type I quasars.

3.4. Fitting result for the relation of C IV EW to the continuum flux

We adopt the maximum likelihood function (equation (3)) based on MCMC to constrain the parameters; the fitting results are shown in Table 2, and the slope of the BEff is $\gamma = -0.164 \pm 0.006$, which suggests that the EW of C IV is inversely correlated with continuum monochromatic luminosities. It is consistent with the result by Bian et al. (2012).

We obtain the distance modulus of Type I quasars by substituting the statistical average values of β and γ into equation (4), which are shown in the upper panel of Fig. 5, including their averages in small redshift bins. Mean-

while the distance modulus and properties of the 471 Type I quasars are listed in Table 1. The lower panel of Fig. 5 shows the plot of the residuals of the distance modulus against redshift; the residuals are from measuring the distance modulus for Type I quasars and Λ CDM cosmology ($\Omega_m = 0.3$). There could be several reasons for the large scatter in the luminosity distance, including observational error, and intrinsic variation of the BEff (Shields 2006; Dietrich et al. 2002). Figure 6 illustrates the diagram of the residuals against the luminosity L_{UV} or the UV-optical power-law index Γ_{UV} . The correlation coefficient for the residuals $\Delta(\log EW(C\text{ IV}))$ and L_{UV} is $r = -0.097$, which represents that $\Delta(\log EW(C\text{ IV}))$ is not correlated with the luminosity L_{UV} . The residuals $\Delta(\log EW(C\text{ IV}))$ is also not relevant with Γ_{UV} ; their correlation coefficient is $r = 0.046$, which implies that the BEff slope has no dependence on L_{UV} or Γ_{UV} in the final sample.

We also consider the relevance of the C IV EW dependence on Eddington ratio L/L_{Edd} and use the relation $\log EW(C\text{ IV}) = \alpha + \beta \log L/L_{Edd}$ to measure luminosity distance for quasars (Baskin & Laor 2004; Bian

Table 1: Properties of the 471 Type I quasars. DM is the distance modulus from a fit of the relation $EW(C\text{ IV}) \propto (\lambda L_\lambda)^\gamma$ with Λ CDM model; σ_{DM} is the error. Only five of the objects are listed.

SDSS name	z	m_r mag	$EW(C\text{ IV})$ \AA	$\log f_\nu(2500\text{\AA})$ $\text{erg s}^{-1}\text{cm}^{-2}\text{Hz}^{-1}$	Γ_{UV}	DM	σ_{DM}
143112.39+093915.4	7.011	21.094 \pm 0.047	26.56 \pm 0.97	-24.536 \pm 0.019	2.964	49.389	1.956
112310.06+134622.5	6.038	21.06 \pm 0.038	27.49 \pm 1.13	-24.505 \pm 0.015	4.383	49.077	1.949
115132.69+550317.3	5.338	21.166 \pm 0.054	28.96 \pm 1.68	-24.534 \pm 0.022	3.823	48.789	1.959
125718.02+374729.9	4.745	20.757 \pm 0.037	29.16 \pm 0.48	-24.358 \pm 0.015	5.042	48.302	1.904
131808.44+215437.0	4.258	20 \pm 0.032	28.06 \pm 0.58	-24.043 \pm 0.013	4.245	47.78	1.886

et al. 2012; Ge et al. 2016). The virial black hole (BH) Masses M_{BH} or Eddington ratio L/L_{Edd} can be estimated from C IV emission lines (Shen et al. 2008, 2011) by formula $\log(M_{BH}/M_\odot) = a + b \log(\lambda L_\lambda/(10^{44} \text{ erg s}^{-1})) + 2 \log(FWHM/(km s^{-1}))$, which is derived from the so-called virial black hole mass estimate $M_{BH} = G^{-1}R_{BLR}V_{BLR}^2$ and $R_{BLR} - \lambda L_\lambda$ relation, and $a = 0.66$, $b = 0.53$ for C IV estimators (McLure & Dunlop 2004; Vestergaard & Peterson 2006). Then we can obtain Eddington ratios L/L_{Edd} , where $L_{Edd} = 1.3 \times 10^{38}(M_{BH}/M_\odot) \text{ erg s}^{-1}$ is the Eddington luminosity. We use the C IV EW- L/L_{Edd} relation to measure the luminosity distance for Type I quasars. Nonetheless, there are even greater errors in the luminosity distance than the results from the C IV EW-luminosity relation $EW(C\text{ IV}) \propto (\lambda L_\lambda)^\gamma$. Therefore, we only use the distance modulus for Type I quasars obtained from C IV Beff and SNIa Pantheon to test the property of dark energy in Section 5.

4. Analysis of the relation $EW(C\text{ IV}) \propto (\lambda L_\lambda)^\gamma$ as a function of z

We divide the Type I quasar data into several redshift bins, which can be used to check if relation $EW(C\text{ IV}) \propto (\lambda L_\lambda)^\gamma$ depends on redshift. The redshift bins satisfy $\Delta(1/(1+z)) = 0.033$. We adopt the parametric model

$$\log EW(C\text{ IV}) = \beta(z) + \gamma(z) \log(\lambda f_\lambda(2500 \text{ \AA})), \quad (6)$$

where $\gamma(z)$ and the intrinsic dispersion $\delta(z)$ are free parameters, and $\beta(z)$ is obtained from equation (2) and can also be a free parameter. We apply segmented Type I quasars data to fit $\gamma(z)$ as well as test whether there is a dependency upon redshift. The fit results of $\gamma(z)$ and $\delta(z)$ at different redshifts are illustrated in Fig. 7; it is easy to see that their values do not obviously deviate from the average, which shows there is no obvious evidence for any significant redshift evolution. The average values of parameter is $\langle \gamma \rangle = -0.154 \pm 0.009$.

5. The reconstruction of dark energy equation of state $w(z)$

Although dark energy can be used to effectively explain the accelerating expansion of the universe and the cosmic microwave background (CMB) anisotropies (Riess et al. 1998; Amanullah et al. 2010; Betoule et al. 2014; Scolnic et al. 2018; Conley et al. 2010; Hu & Dodelson 2002; Ade et al. 2016), the origin and property of its density and pressure remain unclear.

Dark energy can be researched using two main methods. One is to constrain dark energy physical models from observational data and try to explain the physical origin of its density and pressure (Peebles & Ratra 2003; Ratra & Peebles 1988; Li 2004; Maziashvili 2007; Amendola 2000; Gao et al. 2017). Understanding the physical origin of dark energy is important for our universe. It is necessary to determine whether the dark energy is composed of Boson pairs in a vacuum, Fermion pairs, or the Higgs field, and whether it has weak isospin, which may determine whether it can be detected directly in the laboratory. The other method is to study the properties of dark energy, focusing on whether or not its density evolves with time. This can be tested by reconstructing the dark energy equation of state $w(z)$ (Linder 2003; Maor et al. 2002), which does not depend on physical models. High-redshift observational data such as quasars can better solve these issues.

The reconstruction of the equation of state of dark energy $w(z)$ includes parametric and non-parametric methods (Huterer & Starkman 2003; Clarkson & Zunckel 2010; Holsclaw et al. 2010; Seikel et al. 2012; Crittenden et al. 2009; Zhao et al. 2012). We employ Type I quasars and Type Ia supernova (SNIa) to reconstruct $w(z)$ by the parametric method assuming C IV EW-luminosity relation Equation (2), which can be used to test the nature of dark energy.

For SNIa data, the Pantheon sample contains 1048 SNIa from the Pan-STARRS1 (PS1), the Sloan Digital Sky Survey (SDSS), SNLS, and various low- z and Hubble Space Telescope samples. There are 279 SNIa provided by PS1 (Scolnic et al. 2018), and SDSS presented 335 SNIa (Betoule et al. 2014; Gunn et al. 2006; Sako et al. 2018). The rest of the Pantheon sample are from the CfA1-4, CSP, and Hubble Space Telescope (HST) SN surveys (Amanullah et al. 2010; Conley et al. 2010). This combined sample of 1048 SNIa is called the Pantheon sample.

The integral formula of the luminosity-redshift relation in flat space can be written as (Linder 2003; Sahni & Starobinsky 2006)

$$D_L = \frac{1+z}{H_0} \int_0^z dz' [\Omega_m(1+z')^3 + \Omega_R(1+z')^4 + \Omega_{DE}^{(0)} e^{\int_0^{z'} \frac{1+w(z'')}{1+z''} dz''}]^{-1/2}, \quad (7)$$

where Ω_R , Ω_m , and $\Omega_{DE}^{(0)}$ are the present radiation density, matter density, and dark energy density and satisfies $\Omega_{DE}^{(0)} = 1 - \Omega_m$ when ignoring Ω_R , $w(z)$ is the dark energy equation of state. We adopt the parametric form for $w(z)$

$$w(z) = w_0 + w_a \frac{z}{1+z}. \quad (8)$$

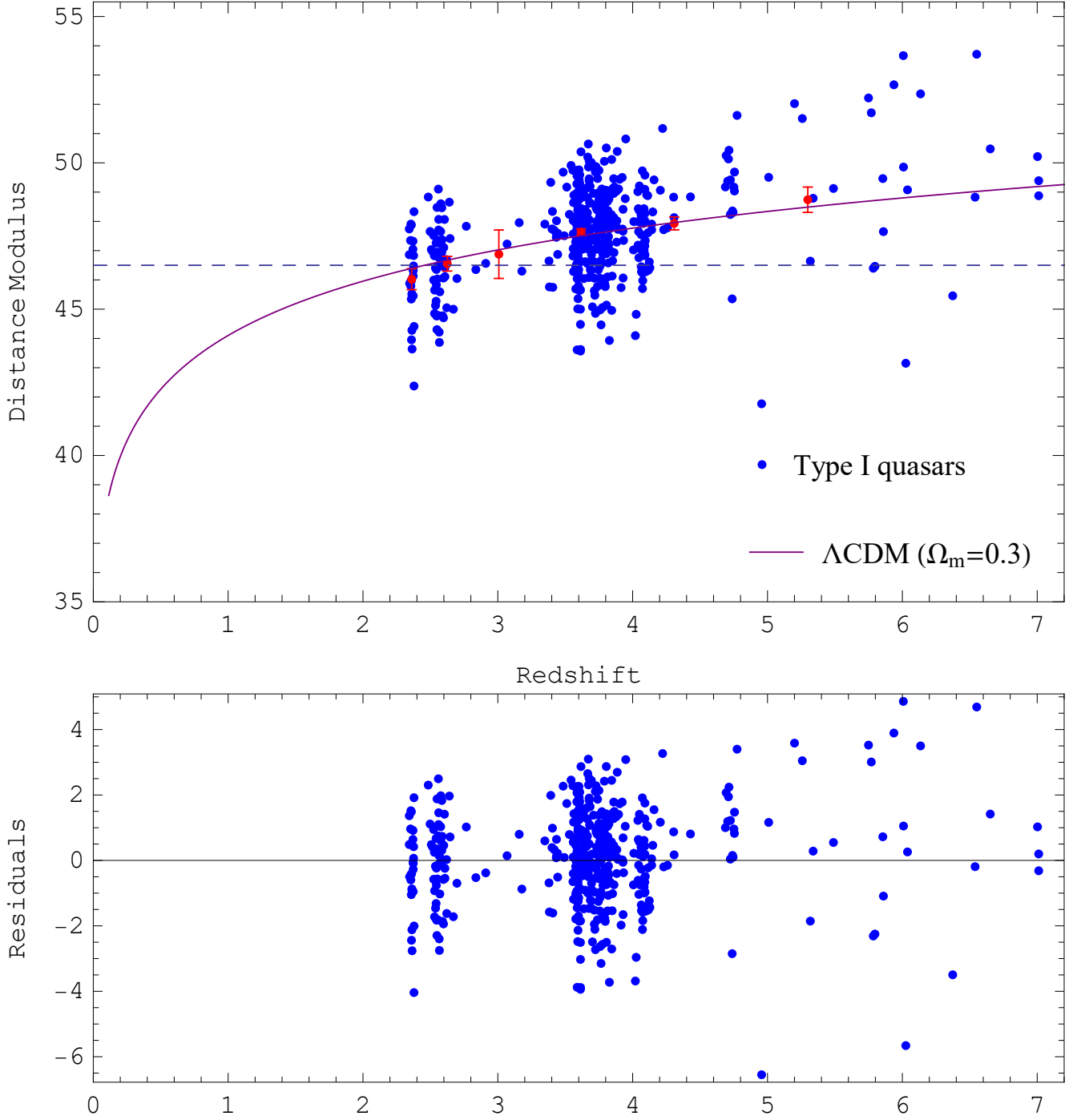


Fig. 5: Type I quasar distance modulus (blue points) from a fit of Equation (2) when assuming Λ CDM cosmology. The red points and bars (upper panel) are distance modulus averages and the standard deviations of the mean in small redshift bins. The purple line shows a flat Λ CDM model fit with $\Omega_m = 0.3$; the dotted line is the reference distance modulus and its value is 46.5. The lower panel shows the residuals of the distance modulus at different redshifts.

Table 2: Fit results on model parameters for a combination of Type I quasars and SNIa

	Parameter	β	γ	δ	Ω_m	w_0	w_α	$\chi'^2_{Total}/\chi^2_{Total}/N$
Λ CDM	<i>Sample</i>			<i>Quasars(Type I)</i>				
	Best Fit	8.84	-0.16	0.092	0.268	—	—	-902.9/475.9/471
	Mean	8.89 ± 0.031	-0.164 ± 0.006	0.103 ± 0.004	0.23 ± 0.01	—	—	
Λ CDM				<i>SN + Quasars(Type I)</i>				
	Best Fit	8.756	-0.158	0.092	0.273	—	—	134.1/1512.9/1519
	Mean	8.734 ± 0.03	-0.158 ± 0.006	0.092 ± 0.003	0.269 ± 0.006	—	—	
$w_0 w_\alpha$ CDM	Best Fit	8.71	-0.157	0.092	0.308	-1.13	0.419	130.1/1509/1519
	Mean	8.72 ± 0.024	-0.157 ± 0.006	0.092 ± 0.003	0.295 ± 0.017	-1.07 ± 0.074	0.108 ± 0.294	

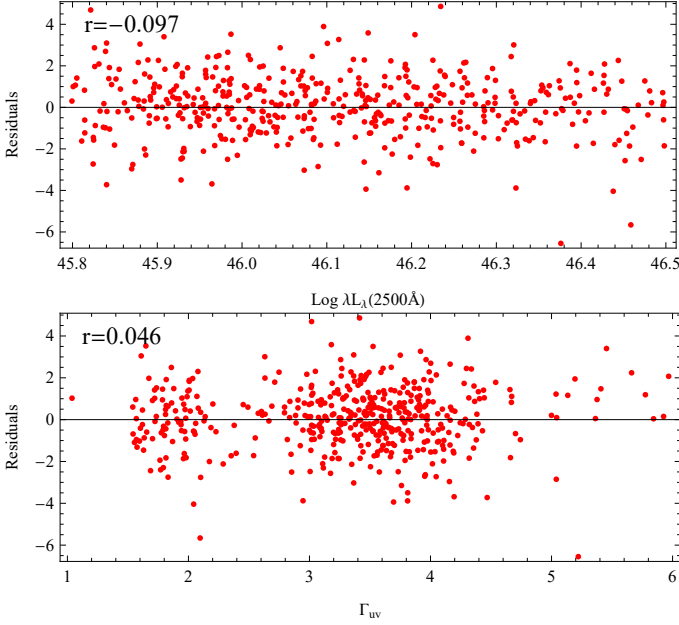


Fig. 6: Plot of residuals of distance modulus against luminosity L_{UV} or UV-optical power-law index Γ_{UV} for the selected sample. This is used to measure the luminosity distance, and r is the correlation coefficient.

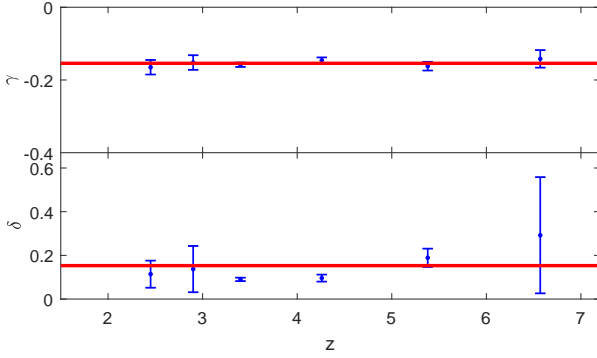


Fig. 7: C IV EW-luminosity correlation in narrow redshift intervals. The blue points are the fit results of $\gamma(z)$, $\delta(z)$ at different redshifts. The horizontal lines show their average values.

and denote it w_0w_aCDM . Therefore dark energy density is

$$\Omega_{DE}(z) = \Omega_{DE}^{(0)}(1+z)^{3(1+w_0+w_a)} \exp[-3w_az/(1+z)]. \quad (9)$$

We constrain the w_0w_aCDM model parameters for Type I quasars and SNIa by minimizing a modified χ'^2_{Total} function. The χ'^2_{Total} is

$$\chi'^2_{Total} = -2 \ln L^{Quasars} + \chi^2_{SN}, \quad (10)$$

where $-2 \ln L^{Quasars}$ is given by equation (3), and χ^2_{SN} can be expressed as

$$\chi^2_{SN} = \Delta\mu^T C_{\mu_{ob}}^{-1} \Delta\mu, \quad (11)$$

where $\Delta\mu = \mu - \mu_{th}$; C_μ is the covariance matrix of the distance modulus μ ; χ'^2_{Total} function also satisfies

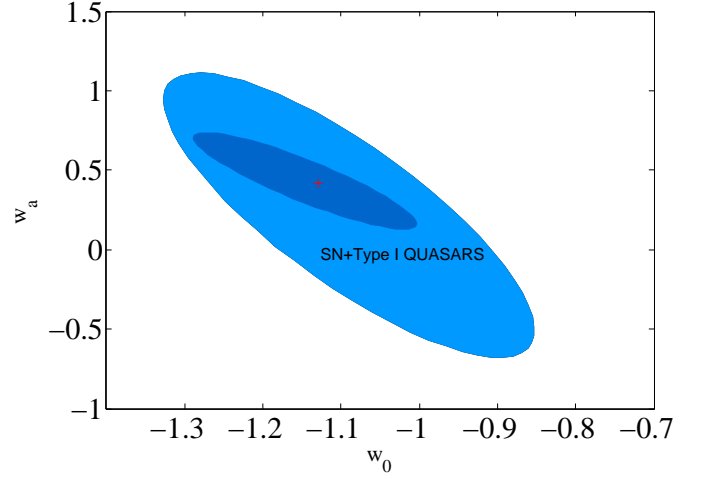


Fig. 8: Contours at 68% and 95% ($\Delta\chi^2 = 1.5, 6$) for w_0 and w_a from a fit of the relation $EW(C\text{ IV}) \propto (\lambda L_\lambda)^\gamma$ with w_0w_aCDM model to a combination of SNIa and Type I quasars. The plus sign (+) in the corresponding color represents the best fitting values for w_0 , w_a .

$$\chi'^2_{Total} = \chi^2_{Quasars} + \chi^2_{SN}; \text{ and } \chi^2_{Quasars} = -2 \ln L^{Quasars} - \sum_{i=1}^N \ln(2\pi s_i^2).$$

We use Type I quasars and SNIa to fit the equation (10) and obtain the statistical results for the cosmological parameters, and their mean and best fit values are listed in Table 2. When using a combination of Type I quasars and SNIa which covers low- and high-redshift data, the results show w_0w_aCDM has better goodness of fit than ΛCDM , and χ'^2_{Total} is improved by -3.9 , which indicates that the ΛCDM model is in tension with Type I quasars and SNIa at $\sim 1.5\sigma$. The results are consistent with the values from radio-loud quasars (Huang & Chang 2022). Meanwhile, Fig. 8 illustrates the 68% and 95% contours for w_0 and w_a from a combination of SNIa and Type I quasars, assuming the C IV EW-luminosity relation $EW(C\text{ IV}) \propto (\lambda L_\lambda)^\gamma$.

6. Summary

Although the precise physical reason for the connection between the EW of C IV and continuum luminosity for quasars is not clearly understood, we can still use a parametric formula to check their correlation. We obtained a sample of 471 Type I quasars with the C IV EW of emission lines and continuum luminosity in the UV-optical band including 25 objects at $5 < z < 7.1$, which can be more effective for checking cosmological model and testing the nature of dark energy. First, we adopted the parametric formula to check the correlation between the C IV EW and luminosity, and obtained a C IV BEff slope $\gamma = -0.164 \pm 0.006$, which implies the EW of C IV is inversely correlated with continuum monochromatic luminosity.

Second, We divided the Type I quasars data into several redshift bins and combined a special model to check if there is a redshift evolution of the C IV EW-luminosity relation. The fitting results show the slope $\gamma(z)$ approaches the constant, which shows that there is not an obvious redshift evolution for $EW(C\text{ IV}) \propto (\lambda L_\lambda)^\gamma$.

Finally, we used a combination of Type I quasars and SNIa to test the property of dark energy by reconstructing the equation of state $w(z)$. The 471 high-redshift Type I quasars included 25 objects at $5 < z < 7.1$, which can be applied to check the cosmological model and test the nature of dark energy more efficiently. The results show the $w_0 w_a$ CDM model is superior to the cosmological constant Λ CDM model at $\sim 1.5\sigma$.

In the future, we will select more Type I quasars at high redshift ($z > 5$) with the C IV 1549 Å emission line and the continuum luminosity from the SDSS quasar catalogs, and hope to obtain $z > 7$ quasars from future optical observations, such as the James Webb Space Telescope (JWST) (Naidu et al. 2022). The high-redshift observational data can be better used to reconstruct the equation of state and test the properties of dark energy, which involves whether or not the universe will keep expanding.

Acknowledgements. This work was supported by the National Natural Science Foundation of China (No.12203029).

References

- Ade, P., Aghanim, N., Arnaud, M., et al. 2016, A&A, 594, A24
- Aghanim, N., Akrami, Y., Ashdown, M., et al. 2020, A&A, 641, A6
- Ahumada, R., Prieto, C. A., Almeida, A., et al. 2020, APJS, 249, 3
- Alam, S., Albareti, F. D., Prieto, C. A., et al. 2015, APJS, 219, 12
- Amanullah, R., Lidman, C., Rubin, D., et al. 2010, APJ, 716, 712
- Amendola, L. 2000, Phys. Rev. D, 62, 043511
- Baldwin, J. A. 1977, APJ, 214, 679
- Baskin, A. & Laor, A. 2004, MNRAS, 350, L31
- Berk, D. E. V., Richards, G. T., Bauer, A., et al. 2001, APJ, 122, 549
- Betoule, M., Kessler, R., Guy, J., et al. 2014, A&A, 568, A22
- Bian, W.-H., Fang, L.-L., Huang, K.-L., & Wang, J.-M. 2012, MNRAS, 427, 2881
- Chang, N., Xie, F., Liu, X., et al. 2021, MNRAS, 503, 1987
- Clarkson, C. & Zunckel, C. 2010, Phys. Rev. Lett., 104, 211301
- Condon, J. J., Cotton, W., Greisen, E., et al. 1998, APJ, 115, 1693
- Conley, A., Guy, J., Sullivan, M., et al. 2010, APJS, 192, 1
- Crittenden, R. G., Pogosian, L., & Zhao, G. B. 2009, JCAP, 2009, 025
- Croom, S., Rhoads, K., Corbett, E., et al. 2002, MNRAS, 337, 275
- Dietrich, M., Hamann, F., Shields, J., et al. 2002, APJ, 581, 912
- Dong, X.-B., Wang, T.-G., Wang, J.-G., et al. 2009, APJ, 703, L1
- Dultzin, D., Marziani, P., De Diego, J., et al. 2020, Frontiers in Astronomy and Space Sciences, 6, 80
- Gao, Z. F., Wang, N., Shan, H., Li, X. D., & Wang, W. 2017, APJ, 849, 19
- Ge, X., Bian, W. H., Jiang, X. L., Liu, W. S., & Wang, X.-F. 2016, MNRAS, 462, 966
- Gunn, J. E., Siegmund, W. A., Mannery, E. J., et al. 2006, AJ, 131, 2332
- Helfand, D. J., White, R. L., & Becker, R. H. 2015, APJ, 801, 26
- Holsclaw, T., Alam, U., Sanso, B., et al. 2010, Phys. Rev. Lett., 105, 241302
- Hu, W. & Dodelson, S. 2002, ARA&A, 40, 171
- Huang, L. & Chang, Z. 2022, MNRAS, 515, 1358
- Huterer, D. & Starkman, G. 2003, Phys. Rev. Lett., 90, 031301
- Kellermann, K., Sramek, R., Schmidt, M., Green, R., & Shaffer, D. 1994, AJ, 108, 1163
- Kellermann, K., Sramek, R., Schmidt, M., Shaffer, D., & Green, R. 1989, AJ, 98, 1195
- Kim, A. G. 2011, PASP, 123, 230
- Kinney, A., Rivolo, A., & Koratkar, A. 1990, APJ, 357, 338
- Kondo, Y., Boggess, A., & Maran, S. P. 1989, ARA&A, 27, 397
- La Franca, F., Bianchi, S., Ponti, G., Branchini, E., & Matt, G. 2014, APJL, 787, L12
- Li, M. 2004, Phys. Lett. B, 603, 1
- Linder, E. V. 2003, Phys. Rev. Lett., 90, 091301
- Lyke, B. W., Higley, A. N., McLane, J., et al. 2020, APJS, 250, 8
- Maor, I., Brustein, R., McMahon, J., & Steinhardt, P. J. 2002, Phys. Rev. D, 65, 123003
- Martínez-Aldama, M. L., Czerny, B., Kawka, D., et al. 2019, APJ, 883, 170
- Maziashvili, M. 2007, Int. J. Mod. Phys. D, 16, 1531
- McLure, R. J. & Dunlop, J. S. 2004, MNRAS, 352, 1390
- Naidu, R. P., Oesch, P. A., van Dokkum, P., et al. 2022, arXiv:2207.09434
- Netzer, H., Laor, A., & Gondhalekar, P. 1992, MNRAS, 254, 15
- Nikolajuk, M. & Walter, R. 2012, MNRAS, 420, 2518
- Pâris, I., Petitjean, P., Aubourg, É., et al. 2012, A & A, 548, A66
- Pâris, I., Petitjean, P., Rollinde, E., et al. 2011, A & A, 530, A50
- Pâris, I., Petitjean, P., Ross, N. P., et al. 2017, A&A, 597, A79
- Peebles, P. J. E. & Ratra, B. 2003, Rev. Mod. Phys. 75, 559
- Ratra, B. & Peebles, P. J. 1988, Phys. Rev. D, 37, 3406
- Reid, M., Pesce, D. W., & Riess, A. 2019, APJL, 886, L27
- Riess, A. G., Filippenko, A. V., Challis, P., et al. 1998, AJ, 116, 1009
- Risaliti, G. & Lusso, E. 2015, APJ, 815, 33
- Sahni, V. & Starobinsky, A. 2006, INT J MOD PHYS D, 15, 2105
- Sako, M., Bassett, B., Becker, A. C., et al. 2018, Publ. Astron. Soc. Aust., 130, 064002
- Scolnic, D. M., Jones, D., Rest, A., et al. 2018, APJ, 859, 101
- Seikel, M., Clarkson, C., & Smith, M. 2012, J. Cosmol. Astropart. Phys., 2012, 036
- Shemmer, O. & Lieber, S. 2015, APJ, 805, 124
- Shen, Y., Greene, J. E., Strauss, M. A., Richards, G. T., & Schneider, D. P. 2008, APJ, 680, 169
- Shen, Y. & Ho, L. C. 2014, Nature, 513, 210
- Shen, Y. & Ménard, B. 2012, APJ, 748, 131
- Shen, Y., Richards, G. T., Strauss, M. A., et al. 2011, APJS, 194, 45
- Shields, J. C. 2006, arXiv preprint astro-ph/0612613
- Stoeckel, J. T., Morris, S. L., Weymann, R. J., & Foltz, C. B. 1992, APJ, 396, 487
- Strittmatter, P., Hill, P., Pauliny-Toth, I., Steppe, H., & Witzel, A. 1980, A&A, 88, L12
- Sulentic, J., Marziani, P., & Dultzin-Hacyan, D. 2000, ARA&A, 38, 521
- Sulentic, J. W., Bachev, R., Marziani, P., Negrete, C. A., & Dultzin, D. 2007, APJ, 666, 757
- Tacconi, L. J., Genzel, R., Saintonge, A., et al. 2018, APJ, 853, 179
- Urry, C. M. & Padovani, P. 1995, Publ. Astron. Soc. Aust., 107, 803
- Vestergaard, M. & Peterson, B. M. 2006, APJ, 641, 689
- Xu, Y., Bian, W. H., Yuan, Q.-R., & Huang, K. L. 2008, MNRAS, 389, 1703
- Zhao, G.-B., Crittenden, R. G., Pogosian, L., & Zhang, X. 2012, Phys. Rev. Lett., 109, 171301
- Zheng, W., Kriss, G. A., & Davidsen, A. F. 1995, APJ, 440, 606